International Journal of Earth, Energy and Environmental Sciences
ISSN: 2517-942X
Vol:9, No:3, 2015

Combining ASTER Thermal Data and Spatial-Based Insolation Model for Identification of Geothermal Active Areas

Khalid Hussein, Waleed Abdalati, Pakorn Petchprayoon, Khaula Alkaabi

***Abstract*—**In this study, we integrated ASTER thermal data with an area-based spatial insolation model to identify and delineate geothermally active areas in Yellowstone National Park (YNP). Two pairs of L1B ASTER day- and nighttime scenes were used to calculate land surface temperature. We employed the Emissivity Normalization Algorithm which separates temperature from emissivity to calculate surface temperature. We calculated the incoming solar radiation for the area covered by each of the four ASTER scenes using an insolation model and used this information to compute temperature due to solar radiation. We then identified the statistical thermal anomalies using land surface temperature and the residuals calculated from modeled temperatures and ASTER-derived surface temperatures. Areas that had temperatures or temperature residuals greater than 2σ and between 1σ and 2σ were considered ASTER-modeled thermal anomalies. The areas identified as thermal anomalies were in strong agreement with the thermal areas obtained from the YNP GIS database. Also the YNP hot springs and geysers were located within areas identified as anomalous thermal areas. The consistency between our results and known geothermally active areas indicate that thermal remote sensing data, integrated with a spatial-based insolation model, provides an effective means for identifying and locating areas of geothermal activities over large areas and rough terrain.

***Keywords*—**Thermal remote sensing, insolation model, land surface temperature, geothermal anomalies.

I. Introduction

SATELLITE remote sensing provides an excellent opportunity to identify thermally active areas that have a high potential to serve as a geothermal energy source. Remote sensing data acquired by thermal sensors onboard different platforms have been used to locate areas of geothermal activity [1]-[5]. The determination of surface temperatures from satellite thermal infrared (TIR) measurements -the primary goal of such sensors- has been complicated by the fact that thermal infrared radiances observed by satellites are not uniquely dependent on temperature, but rather vary with both temperature and emissivity [6].

Since, the emissivity of water is well defined, the TIR remote sensing data have been used very effectively to measure and monitor sea surface temperature [7]-[13]. If the same techniques applied to retrieve sea surface temperature are used for the recovery of land surface temperature, however, large errors occur because the emissivity of the surface is unknown. Therefore, studies that require accurate land surface temperature are largely limited to those cases where the surface emissivity is well known [14]. Various techniques have been developed, however, that separate temperature and emissivity in the multispectral thermal infrared wavelengths. Among these are the reference channel, the emissivity normalization, and the alpha derived emissivity, and these techniques differ based on the assumptions they make [6], [14]-[18]. The reference channel method assumes a constant emissivity value for a certain channel and uses this emissivity to calculate the temperature of this channel and then the temperature is used to calculate the emissivity of the other channels. Then the emissivities are used to calculate the surface temperature. The emissivity normalization method resembles the reference channel, except the constant emissivity value is used for each channel and the highest temperature is assigned to the pixel and used to calculate the emissivity. Alpha derived emissivity technique is based on Wien's approximation of the Plank function.

Land surface temperature of geothermally active areas is composed of two components, temperature due to solar radiation absorbed by the surface which is influenced by elevation as well as surface orientation (slope and aspect), and temperature as a result of geothermal heat. Therefore, it is difficult to separate between the temperature anomalies due to solar radiation and topographic effects, and anomalies due to geothermal heat. Recently, numerous studies have suggested some techniques and methods to compensate for solar and topographic effects. For example, [1] mapped surface temperature anomalies associated with geothermal activity at Bradys Hot Springs, Nevada, USA, by processing the Advanced Spaceborne Thermal Emission Reflection Radiometer (ASTER) thermal data to minimize the albedo, slope and diurnal heat effects. They corrected for albedo and slope using the visible and near infrared bands of ASTER and a digital elevation model, respectively. The diurnal heat effects were corrected using 24 hours surface temperature

Khalid Hussein is with Cooperative Institute for Research in Environmental Sciences (CIRES), University of Colorado, Boulder, CO 80309 USA. He is now with the Department of Geography and Urban Planning, United Arab Emirates University, Al Ain, P. O. Box 15551, UAE (e-mail: khalid.hussein@uaeu.ac.ae).

Waleed Abdalati is with Cooperative Institute for Research in Environmental Sciences (CIRES), University of Colorado, Boulder, CO 80309 USA (e-mail: waleed.abdalati@colorado.edu).

Pakorn Petchprayoon is with Geo-Informatics and Space Technology Development Agency, Bangkok, 10210, Thailand (e-mail: pakorn@gistda.or.th).

Khaula Alkaabi is with the Department of Geography and Urban Planning, United Arab Emirates University, Al Ain, P. O. Box 15551, UAE (e-mail: khaula.alkaabi@uaeu.ac.ae).

measurements in integration with ASTER day- and nighttime data. A simple energy balance assuming the latent heat flux is negligible was used. Their method is suited for dry or desert areas like Nevada; however it is difficult to apply such a method in moist and vegetated areas. Moreover, the method needs a pair of day- and nighttime data, for the same day and such pairs are limited in availability, particularly for large areas. An alternative to that are spatially-based models that compute the spatial and temporal variations of the incoming solar radiation (insolation).

Spatial insolation models can be categorized into two types [19], point specific and area based. Point specific models calculate insolation for a location, while area based calculate insolation for a geographic area. Fu and Rich [19] developed the Solar Analyst©, a geometric solar radiation model that calculates the amount of the incoming solar radiation, which is utilized in different fields including, forestry, civil engineering, agriculture, ecology, and environmental assessment [20]. The model creates an upward looking hemispherical viewsheds which are used to compute the solar insolation for each location and produce accurate insolation maps. The model uses a digital elevation model as a major input and takes into account location latitude and altitude, surface slope and aspect, shadows cast surrounding topography, daily and seasonal shifts in solar angle, and atmospheric attenuation.

In this study, we explore the possibility of using ASTER thermal data in conjunction with an area based spatial insolation model developed by Fu and Rich [19] to identify and delineate areas of geothermal activity. The specific objectives of this study are to: (i) compute insolation of the same area covered by the ASTER scene and convert the insolation to temperature, (ii) calculate land surface temperature from ASTER thermal data using one of temperature emissivity separation (TES) algorithms, and (iii) determine the geothermal temperature as a residual of model temperature and ASTER surface temperature and use it to locate and identify areas of geothermal activity.

II. Study Area and Data

The study area is located in Yellowstone National Park (YNP) which extends into Wyoming, Montana, and Idaho States in the U.S. A. and occupies 8900 km2. YNP is situated on a high plateau (2400 m average elevation) along the continental divide between the Northern and the Middle Rocky Mountains [21]. The elevation of the mountains varies from 3000 m to 4250 m. The mountains include Madison Range to the west, the Gallatin and Beartooth Mountains to the north, the Absaroka Mountains to the east, and the Teton Range to the south (Fig. 1).

The YNP is known for its geothermal features such as Norris Mammoth Corridor and Gibbon Canyon, thus it has been chosen to test the use of remotely sensed thermal data and solar radiation model for identification and delineation of geothermal active areas. In this study, we used data acquired by ASTER. ASTER is a multispectral sensor launched onboard Terra platform of NASA in 1999 and it obtains high-resolution (15 to 90 meters per pixel) images of the Earth in 14 different wavelengths, ranging from visible to thermal infrared parts of the electromagnetic spectrum. Two pairs of L1B ASTER nighttime scenes acquired during May, 2011 and daytime scenes acquired in May, 2012 were downloaded from EROS Data Center. Daytime data were not available for the same dates as the nighttime data. The two scenes cover most area of the YNP. The thermal images were georectified and corrected for atmospheric effects. The United States Geological Survey (USGS) 30m resolution Digital Elevation Model (DEM) is used to compute the incoming solar radiation based on slope and aspect characteristics of the location. To validate the results of this study, a thermal area shape file was obtained from the YNP GIS database for comparison.

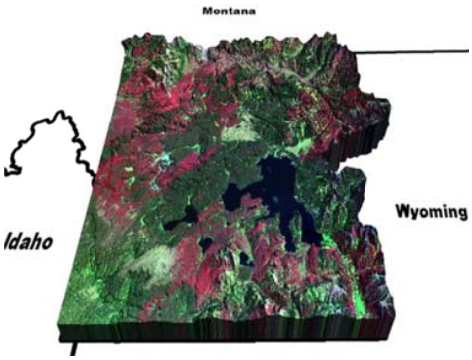

Fig. 1 Digital terrain model showing the location and the topographic characteristics of Yellowstone National Park. Yellowstone Lake appears as dark blue in the right center

III. Methodology

A. Retrieval of Insolation

The Solar Analyst© model, developed by Fu and Rich [19], is used to calculate the incoming clear sky conditions solar radiation for the area covered by each of the four ASTER scenes. The model computes the insolation for the day or part of the day during which the ASTER scenes were acquired. The model creates an upward looking hemispherical viewshed (the angular distribution of sky obstruction) for every location on the DEM. The hemispherical viewsheds are then used to calculate the insolation for each location and to produce insolation map. The model calculates a viewshed by searching in a specified set of directions around a location of interest determining the maximum angle of obstruction (horizon angle) in each direction. Then the horizon angles are converted into a hemispherical coordinate system. The viewshed grid cell is identified with visible or obstructed sky directions. The grid cell location (row and column) corresponds to zenith and azimuth angles. The model divides the whole sky into a series of sky sectors defined by zenith and azimuth angles. Homogenous transmissivity and diffuse proportion parameters were used, because the ASTER scenes were approximately free of clouds. The total solar radiation is composed of three components, direct, diffuse, and reflected. Hence, the reflected radiation from surroundings generally

accounts for a small portion of the global radiation; the model computes the direct and diffuse components.

The direct solar radiation is calculated as a function of sun position at interval of half an hour through the day. The position of the sun is calculated based on latitude, day of the year during which the scenes were acquired, and time of the day. The model takes into account the penumbral effects. The total direct radiation for a ground location is computed as the sum of direct radiation from all sky directions. The direct radiation of sky direction with a zenith angle θ and azimuth angle α is calculated using (1):

$$DirIns_{\theta,\alpha} = S_{const} * \tau^{m(\theta)} * SunDur_{\theta,\alpha} * SunGap_{\theta,\alpha} * cos(AngIn_{\theta,\alpha}) \quad (1)$$

where S_{const}= the solar constant (1367 Wm^{-2}); τ= transmittivity of the atmosphere; m= relative optical path length; $SunDur_{\theta,\alpha}$= time duration represented by sky sector; $SunGap_{\theta,\alpha}$= gap; fraction (proportion of unobstructed sky area in each sky sector); $AngIn_{\theta,\alpha}$= angle of incidence between the centroid of the sky sector and the axis normal to the surface. The relative path (m) and AngInθ, α are calculated with (2) and (3), respectively:

$$m = exp(-0.000118 * elev - 1.638 * 10^{-9} * elev^2)/\cos(\theta) \quad (2)$$

$$\mathrm{AngIn}_{\theta,\alpha} = \mathrm{acos}[\cos(\theta) * \cos(G_z) + \sin(\theta) * \sin(G_z) * \cos(\alpha - G_a)] \quad (3)$$

where *elev*= elevation in meters; θ= solar zenith angle; G_z= surface zenith angle; G_a= surface azimuth angle. Solar Analyst© determines the incoming diffuse radiation as uniform, i.e. the same from all sky directions, or the diffuse radiation varies with zenith angle. This study assumed that diffuse radiation flux was uniform over the area covered by ASTER scene. The diffuse radiation is integrated over half an hour interval and corrected by the gap fraction and angle of incidence using (4):

$$DiffIns_{\theta,\alpha} = R_{glob} * P_{diff} * Dur * SkyGap_{\theta,\alpha} * Weight_{\theta,\alpha} * cos(AngIn_{\theta,\alpha}) \quad (4)$$

where R_{glob}= global normal radiation (calculated using (5)); P_{diff}= diffuse proportion of global normal radiation flux; *Dur*= time interval; $SkyGap_{\theta,\alpha}$ = gap fraction (proportion of visible sky) for the sky sector; $Weight_{\theta,\alpha}$= proportion of diffuse radiation originating in a given sky sector relative to all sectors (calculated using (6)); $AngIn_{\theta,\alpha}$= angle of incidence between the centroid of the sky sector and the axis normal to the surface

Global normal radiation (Rglob) is calculated by summing up the direct radiation from every sky sector including the obstructed ones without correcting for angle of incidence and then correcting for proportion of direct radiation (5):

$$R_{glob} = (S_{const} \sum \tau^{m(\theta)})/(1 - P_{diff}) \quad (5)$$

$\mathrm{Weight}_{\theta,\alpha}$ for uniform diffuse radiation is calculated using (6):

$$Weight_{\theta,\alpha} = (cos\theta_2 - cos\theta_1)/Div_{azi} \quad (6)$$

where θ_1, θ_2 = zenith angles bounding the sky sector; Div_{azi}= number of azimuthal division in the sky map.

Total diffuse radiation is computed as the sum of the diffuse solar radiation (DiffIns θ, α) and the global solar radiation is calculated as the sum of direct and diffuse radiation of all sectors.

B. Retrieval of Land Surface Temperature

Land surface of YNP is heterogeneous and in turn has variable emissivities. Therefore, we employ an Emissivity Normalization Algorithm which separates temperature from emissivity to calculate the temperature of each pixel. We used the following steps to calculate surface temperature: (1) assume an emissivity of 0.96 to make an initial temperature calculation for each pixel for the 5 ASTER thermal channels (i.e. each pixel has 5 temperatures); (2) assign the highest temperature from step 1 as the temperature of the pixel and calculate the emissivity of the surface of each channel based on that temperature; (3) using the derived emissivities in step 2, recalculate the emitted radiance (L′) for each band; (4) use the L′ values to recalculate the emissivities of each band and then these new emissivities to recalculate L′ (producing L″); (5) repeat steps 3 and 4 until a convergence threshold of emitted radiance is reached. For details of the algorithm see [6].

C. Identification of Thermal Anomalies

Calculated temperatures were used to identify and delineate the geothermal areas. Since, the model does not take into account the radiation reflected to the surface and the land surface temperature is a result of the solar radiation of multiple days and the physical properties of the surface, we identified the thermal anomalies statistically. We calculated the mean temperature and the standard deviation (σ) of the temperature and temperature residuals of each scene in order to identify areas that have temperatures, between mean plus 1σ and mean plus 2σ, and greater than mean plus 2σ. The temperature distribution of one of the nighttime images is shown in Fig. 2. Areas that had temperature or temperature residual greater than 2σ and between 1σ and 2σ, were considered ASTER modeled very warm and warm surface exposures (thermal anomalies), respectively. Assuming there is some geothermal activity somewhere in the scene, we identify these locations with values greater 2σ as likely sources of such flux.

IV. Results

The integration of remotely sensed thermal data with a solar radiation model reduced topographic effects significantly, and has improved our ability to correctly identify geothermally active areas.

A. Insolation Map

The global insolation (direct and diffuse radiation) map during the day the nighttime data acquired is shown in Fig. 3. Topography, surface slope and aspect, and shadows created by topographic features are the main factors modifying

distribution of the incoming solar radiation, and these lead to high spatial variations in the amount of insolation received by the surface, which in turn results in variability of surface temperature. The warm colors indicate areas that have received high solar radiations and those were areas of gentle slope and/or not obscured by topography and areas facing south. Lower insolation values depicted by cool colors were mostly on the north facing slopes and on areas where the sky is blocked by topography.

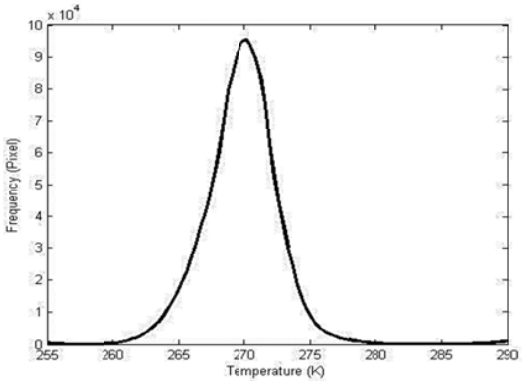

Fig. 2 Temperature distribution of one of the nighttime scenes

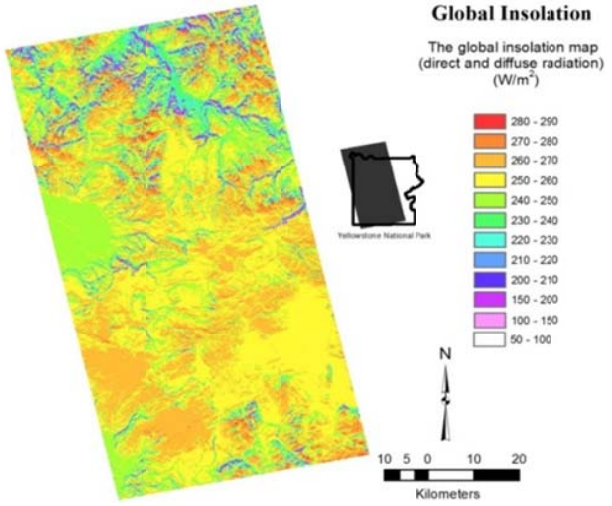

Fig. 3 Map of the global insolation received by the surface during the day ASTER nighttime images were acquired

B. Temperature Maps and Thermal Anomalies

Table I shows the statistics of the temperature of the four ASTER scenes calculated using the Emissivity Normalization Algorithm. The temperature of the daytime images show more variability compared to the nighttime data. This is mainly due to the effects of solar geometry and topography.

The temperature results revealed that some portions of the study area had elevated temperatures on surfaces with sun-facing orientations, for example, the areas outlined by boxes (Fig. 4 (a)). However, it was difficult to distinguish between high temperatures due to geothermal activity and those caused by other sources such as solar radiation and surface orientation effects. To correct for topographic and surface orientation effects and under the assumption that the land surface temperature due to solar radiation is mostly generated by the insolation received by the surface during the day that the ASTER scene was acquired, the modeled insolation is converted to temperature using the emissivities (absorptivities) calculated from ASTER data. If the area beneath the surface has geothermal activity, then the residual of temperatures calculated from ASTER thermal data and the modeled insolation composed mostly temperature due to geothermal heat (Fig. 4 (b)). Incorporating insolation model that calculates the spatial variations in the coming solar radiation with ASTER temperature significantly reduced the effects of solar geometry and topography in identifying areas of geothermal activity. Figs. 5 (a) and 6 (a) show that large areas have been erroneously identified as thermal anomalies from ASTER surface temperature data before correction for the incoming solar radiation.

TABLE I
TEMPERATURE (DEGREES KELVIN) STATISTICS OF THE FOUR ANALYZED ASTER SCENES

Scene/Time	Maximum Temperature (°K)	Minimum Temperature (°K)	Mean Temperature (°K)	Standard Deviation (σ)
Upper/Day	319.33	266.10	300.30	10.39
Lower/Day	313.16	270.91	290.91	07.79
Upper/Night	285.86	257.72	272.46	02.68
Lower/Night	288.56	257.81	271.15	02.54

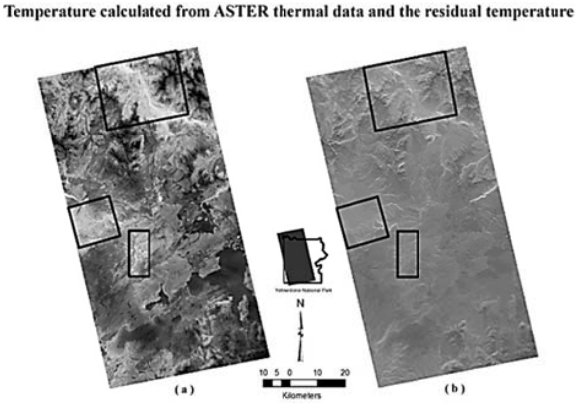

Fig. 4 (a) Temperature calculated from ASTER thermal data, and (b) the residual temperature (boxes show some areas where the topographic and solar effects were eliminated or significantly reduced)

Deriving thermal anomalies from the residual temperature revealed that the effects of topography and surface orientation is reduced significantly as evident by reduction in thermally anomalous areas within each scene (Figs. 5 (b) and 6 (b)). As more evidence of the improvement of the results after application of the model, the Grand Canyon known for its geothermal activity stands out clearly on both night- and daytime data. In our analysis this area initially identified as warm becomes classified as very warm (>2σ) after we account for solar effects. This can be seen in the residual temperatures in Figs. 5 and 6.

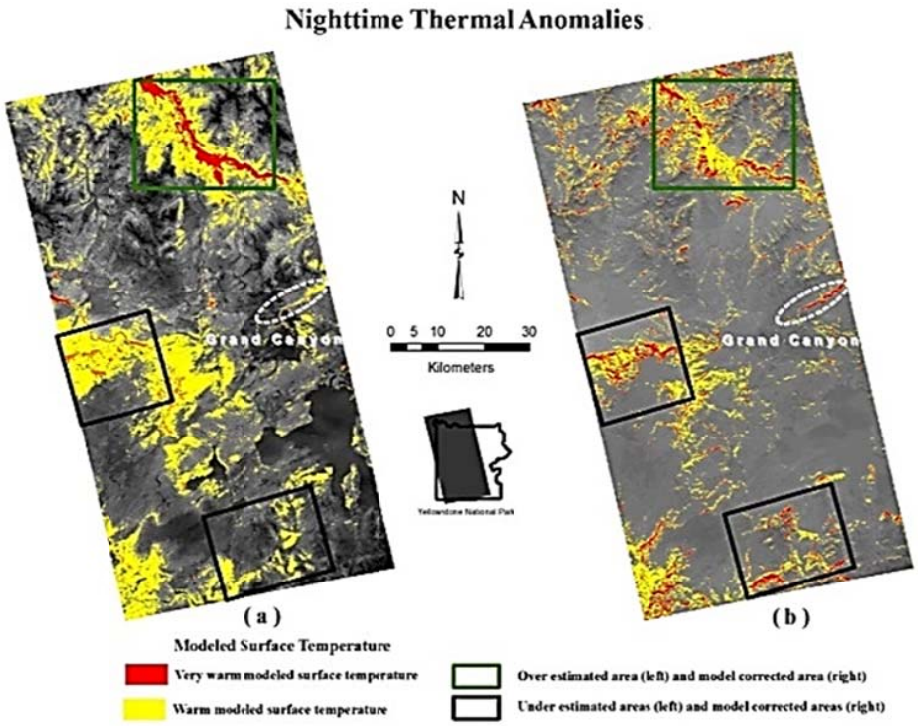

Fig. 5 (a) Thermal anomalies derived from ASTER nighttime surface temperature, and (b) Thermal anomalies derived from the residual temperature (boxes show some areas where the topographic and solar effects were eliminated or significantly reduced)

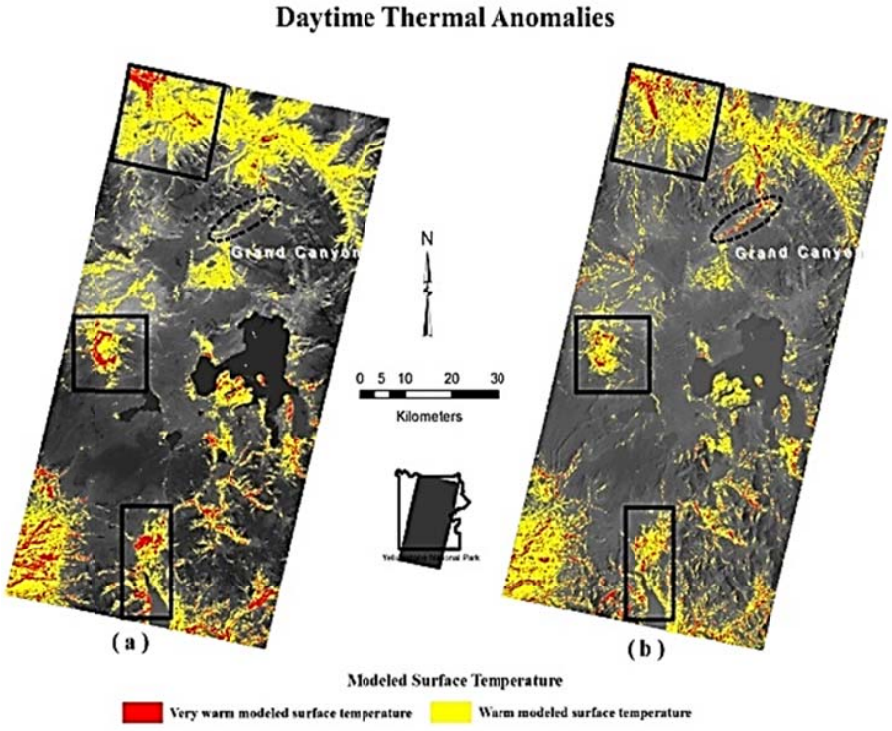

Fig. 6 (a) Thermal anomalies derived from ASTER daytime surface temperature, and (b) Thermal anomalies derived from the residual temperature (boxes show some areas where the topographic and solar effects were eliminated or significantly reduced)

Large areas of geothermal activity have been identified from day- and nighttime data analysis before application of the model, and this obviously an overestimation (green box area, Fig. 5), which are the areas that have received greater

insolation than other areas. However, there were some areas reclassified as having thermal anomalies after incorporating the model results (i.e. they were underestimated before employing the model). This is because the statistics are biased towards areas that have high temperature due to solar and topographic effects (black box, Fig. 5), and the model allows us to compensate for those biases.

The thermal anomalies obtained from the residual temperatures derived from both day- and nighttime data show that geothermal areas of Yellowstone National Park can be identified and delineated (Figs. 7 and 8).

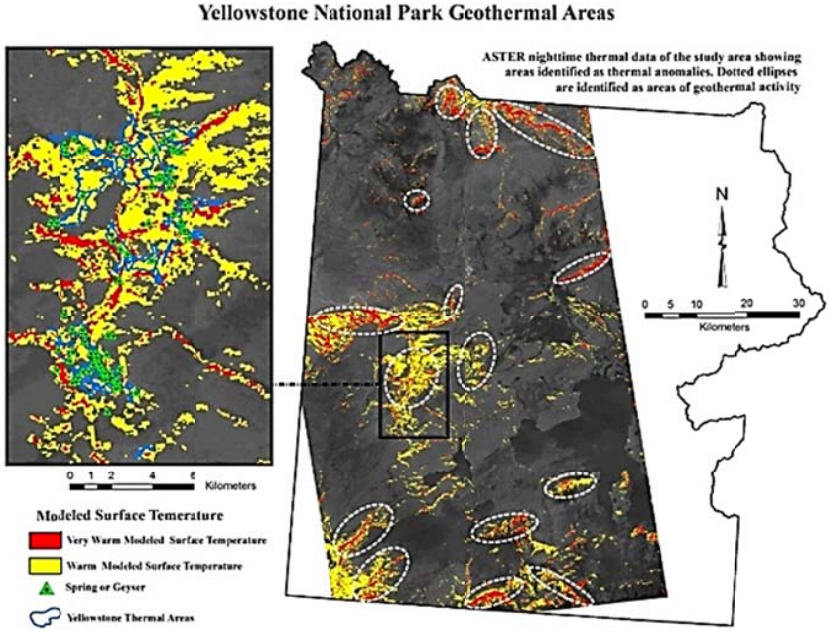

Fig. 7 ASTER nighttime thermal data of the study area showing areas identified as thermal anomalies (dotted ellipses are identified as areas of geothermal activity (right). Lower and Midway thermal areas, springs and geysers superimposed on ASTER nighttime thermal anomalies (left))

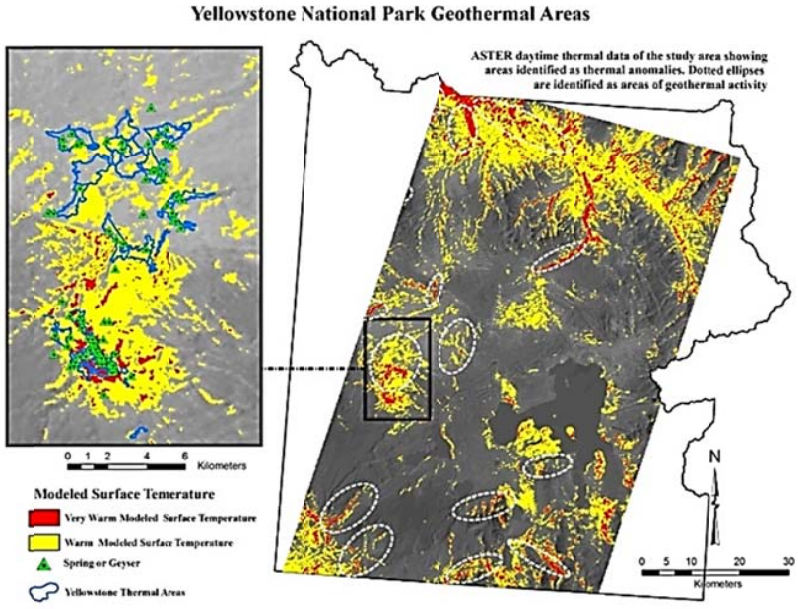

Fig. 8 ASTER daytime thermal data of the study area showing areas identified as thermal anomalies (dotted ellipses are identified as areas of geothermal activity (right). Lower and Midway thermal areas, springs and geysers superimposed on ASTER daytime thermal anomalies (left))

C. Validation of the Results

To validate the results, we compared the areas identified as thermally anomalous to the thermal areas obtained from the YNP GIS database. Also the hot springs and geysers were plotted over the study area. Most of the thermal areas (YNP), springs and geysers are located within our identified anomalous thermal areas (Figs. 7 and 8), for example, the thermal areas located in Midway and Lower basins are shown in Figs. 7 and 8. In some cases, the areas identified by remote sensing thermal data are larger than the YNP areas and may not be geographically matched with it. We believe this is due to geo-referencing errors of ASTER data and/or due to errors in delineation of Yellowstone thermal areas. The YNP thermal areas were delineated based on visual observations of the absence or scarceness of vegetation in or around hydrothermal features, therefore errors may occur in the location of the boundaries. Also thermal areas and/or basins change overtime; thermal area boundaries can grow a meter or more in a month's time [22].

V. Discussion

The results of this study indicate that thermal remote sensing can be used as a key tool in detection and exploration of geothermal areas. However, two major difficulties limit its use; the first one is the accurate retrieval of land surface temperature (LST), and the second is the separation of LST due to incoming solar radiation and topographic effects from LST as a result of geothermal heat.

The radiance emitted from the surface of the Earth in thermal infrared region of electromagnetic spectrum depends on the temperature and the emissivity of the surface. The land surface of YNP has variable chemistry and texture, because it is composed of various land use and land cover types, and thus emissivity is variable. Therefore, calculating temperatures using average emissivity will result in errors of temperature values. However, our use of the temperature emissivity separation algorithm on the five ASTER thermal bands allowed us to accurately calculate land surface temperatures of the study area. This is only possible because we could account for the topographic, atmospheric, and surface orientation effects. using Solar Analyst©, which can create maps of global radiation integrated over any period of time using digital elevation model as an input with few other parameters. The temperature due to geothermal heat is calculated as the residual of the ASTER temperature and the temperature due to incoming solar radiation. This technique, which eliminates or significantly reduces the solar and topographic effects, has advantages over techniques that require day-and nighttime imagery from the same day: (1) it can be applied to large areas using ASTER data given a digital elevation model is available for the area, even in the absence of day- and nighttime image pairs, allowing the analysis of more images. (2) No field data is required to correct for the albedo and topography. (3) No geothermal features (e.g. hot springs) are priori needed to apply the technique, i.e. the technique is very useful in blind geothermal areas.

Our approach does have some limitations, as indicated by some falsely identified geothermally active areas, which most likely result from topographic and surface orientation effects on the incoming solar radiation. There were obviously overestimations in regions that have received greater insolation than other areas. In contrast, there were some underestimated parts caused by the statistics biased towards areas that have high temperature due to solar and topographic effects. However, combining ASTER thermal data with spatial based insolation model has significantly reduced the effects of spatial variation of insolation on identification of geothermal areas. This is evident by the fact that day-and nighttime data produced very similar results in areas where there were overlapped.

VI. Conclusions

The results of this study showed that satellite remote sensing is very useful in detecting and identifying areas of geothermal activity. Thus remote sensing techniques provide a valuable tool for the identification of surface "hot spots" that have a high potential to serve as a geothermal energy source. Spatial insolation models are good tools for estimating the amount of incoming solar radiation received on surfaces of various topography and surface orientation. Therefore, they can be used to eliminate or reduce the surface orientation effects on temperature values calculated from thermal infrared imagery and in turn help in detecting temperature anomalies ascribable to geothermal activity. This technique is one of the first attempts to develop algorithm combines remote sensing information with a spatial-based insolation model to provide a valuable tool for locating areas of geothermal activities over large areas and rough terrain.

Acknowledgment

This study was supported by Department of Energy (DOE) Project-DOE Grant DE-EE0002828 awarded to Flint Geothermal, LLC, Denver. We wish to acknowledge Mr. Mark Ziegenbein, Mr. Grant Logsdon, and Mr. Lee Robinson for their support and cooperation.

References

[1] M. F. Coolbuagh, C. Kratt, A. Fallacaro, W. M. Calvin, and J. V. Taranik, "Detection of geothermal anomalies using Advanced Spaceborne Thermal Emission and Reflection Radiometer (ASTER) thermal infrared images at Brady's Hot Springs, Nevada, USA", Remote Sensing of Environment, vol. 106, pp. 350-359, 2007.

[2] M. Eneva, M.Coolbaugh, S. Bjornstad, and J. Combs, "Detection of surface temperature anomalies in the Coso Geothermal Field using thermal infrared remote sensing. GRC Transaction", vol. 31, pp. 335-340, 2007.

[3] M. Eneva, M. Coolbaugh, and J. Combs, "Application of satellite thermal infrared imagery to geothermal exploration in east central California. GRC Transaction" vol. 30, pp. 407-411, 2006.

[4] M. Eneva, and M. Coolbaugh, "Importance of elevation and temperature inversions for the interpretation of thermal infrared satellite images used in geothermal exploration", GRC Transaction, vol. 33, pp. 467-470, 2009.

[5] R. G. Vaughan, L. P. Keszthelyi, J. B. Lowenstern, C. Jaworowski, and H. Heasler, "Use of ASTER and MODIS thermal infrared data to quantify heat flow and hydrothermal change at Yellowstone National

Park", Journal of Volcanology and Geothermal Research, vol. 233-234, pp. 72-79, 2012.
[6] A. Gillespie, S. Rokugawa, T. Matsunaga, S. J. Cothern, S. Hook, and B. A. Kahle, "A temperature and emissivity separation algorithm for Advanced Spaceborne Thermal Emission and Reflection Radiometer (ASTER) images", IEEE Transactions on Geoscience, vol. 30, no. 4, pp. 1113-1126, 1998.
[7] D. Anding, and R. Kauth, "Estimation of sea surface temperature from space", Remote Sensing of Environment, vol. 1, pp. 217-220, 1970.
[8] I. J. Barton, "Transmission model and ground-truth investigation of satellite derived sea surface temperatures", Climate and Applied Metrology, vol. 24, pp. 508-516, 1985.
[9] A. K. Kilpatrick, P. G., Podestfi, and R. Evans, "Overview of the NOAA/NASA advanced very high resolution radiometer Pathfinder algorithm for sea surface temperature and associated matchup database", Geophysical Research, vol. 106, no. C5, 9179-9197, 2001.
[10] C. D. McConaghy, "Measuring sea surface temperature from satellites. Remote Sensing of Environment", vol. 10, pp. 307-310, 1980.
[11] M. L. McMillin, and S. D. Crosby, "Theory and validation of the multiple window sea surface temperature technique", Geophysical Research, vol. 89, no. C3, pp. 3655-3661, 1984.
[12] E. V. Noble, and C. J. Wilkerson, "Sea surface temperature mapping flights-Norwegian Sea, summer 1968'. Remote Sensing of Environment, vol. 1, pp. 187-193, 1970.
[13] C. Walton, "Satellite measurement of sea surface temperature in the presence of volcanic aerosols. Climate and Applied Meteorology", vol. 24, no. 6, pp. 501-507, 1985.
[14] C. Prabhakara, G. Dalu, and G. V. Kunde, "Estimation of sea surface temperature from remote sensing in the 11- to 13-3μm window region", Geophysical Research vol. 79, no. 33, pp. 5039-5044, 1974.
[15] S. P. Kealy, and J. S. Hook, "Separating temperature and emissivity in thermal infrared multispectral scanner data: Implications for recovering land surface temperatures", IEEE Transactions on Geoscience and Remote Sensing, vol. 31, no. 6, pp. 1155-1164, 1993.
[16] J. S. Hook, R. A. Gabell, A. A. Green, and S. P. Kealy, "A comparison of techniques for extracting emissivity information from thermal infrared data for geologic studies", Remote Sensing of Environment, vol. 42, pp. 123-135, 1992.
[17] S. Tang, Q. Zhu, X. Bai, S. Yang, Y. Shuai, and Q. Bu, "A TES algorithm based on corrected Alpha Difference Spectra" IEEE, pp. 450-4503, 2004.
[18] S. Tang, X. Li, J. Wang, Q. Zhu, and L. Zhang, "An improved TES based on the corrected ALPHA difference spectrum", Science in China Series D-Earth Sciences, vol. 50, no. 2, pp. 274-282, 2007.
[19] P. Fu, and M. P. Rich, Design and implementation of the Solar Analyst: an ArcView extension for modeling solar radiation at landscape scales. Proceedings of the Nineteenth Annual ESRI User Conference, 1999.
[20] P. Fu, and M. P. Rich, "A Geometric Solar Radiation Model with Applications in Agriculture and Forestry. Computers and Electronics in Agriculture", vol. 37, pp. 25–35, 2002.
[21] Spatial Analysis Center, "Yellowstone National Park. Hydrogeothermal Areas of Yellowstone National Park, Wyoming, Montana, Idaho (Unpublished work)", Online-Linkage: \\inpyellgis2\data\yell_data\geothermal\y_thermarea, unpublished.
[22] C. A. Wood, and J. Kienle, "Volcanoes of North America: United States and Canada": Cambridge University Press, contribution by Christiansen, R. L, 354 p, 1990.